



Contents lists available at ScienceDirect

Journal of Rock Mechanics and Geotechnical Engineering

journal homepage: www.rockgeotech.org

Full length article

Improved shape hardening function for bounding surface model for cohesive soils

Andrés Nieto-Leal ^{a,b}, Victor N. Kaliakin ^{a,*}^a Department of Civil & Environmental Engineering, University of Delaware, Newark, DE 19716, USA^b Department of Civil Engineering, Universidad Militar Nueva Granada, Bogotá, Colombia

ARTICLE INFO

Article history:

Received 9 April 2013

Received in revised form

11 December 2013

Accepted 25 December 2013

Available online 4 March 2014

Keywords:

Constitutive model

Bounding surface plasticity

Shape hardening function

Clay

ABSTRACT

A shape hardening function is developed that improves the predictive capabilities of the generalized bounding surface model for cohesive soils, especially when applied to overconsolidated specimens. This improvement is realized without any changes to the simple elliptical shape of the bounding surface, and actually reduces the number of parameters associated with the model by one.

© 2014 Institute of Rock and Soil Mechanics, Chinese Academy of Sciences. Production and hosting by Elsevier B.V. All rights reserved.

1. Introduction

Since the late 1970's, the bounding surface concept has been successfully used to simulate the response of cohesive soils. A form of a bounding surface/yield surface model was briefly mentioned by Mröz et al. (1978) and subsequently fully developed within the framework of critical state soil mechanics by Mröz and his co-workers (Mröz et al., 1979; Pietruszczak and Mröz, 1979).

A direct bounding surface formulation for isotropic soil plasticity was qualitatively presented by Dafalias (1979a) for the case of zero elastic range and in conjunction with implied loading surfaces and a quasi-elastic range (Dafalias, 1979b). The latter version of the model was subsequently developed fully within a two- (Dafalias and Herrmann, 1980, 1982a) and three-invariant framework (Dafalias and Herrmann, 1982b; Dafalias et al., 1982), synthesized (Dafalias and Herrmann, 1986), and then subsequently simplified (Kaliakin and Dafalias, 1989). Anandarajah and Dafalias (1986) developed a version of the model suitable for simulating the

response of anisotropically consolidated cohesive soils that served as a basis for subsequent enhanced anisotropic bounding surface models (Ling et al., 2002; Jiang et al., 2012). A time-dependent version of the model for isotropic cohesive soils was proposed (Dafalias, 1982a,b, 1986a), refined and implemented by Kaliakin (1985), and formally presented and verified (Kaliakin and Dafalias, 1990a,b).

The predictive capabilities of bounding surface models for cohesive soils have typically been assessed by comparing numerical results with data obtained from laboratory tests. The majority of these tests were performed under axisymmetric triaxial compression and extension stress states. In a few instances, more complex stress states were considered. This included the centrifuge modeling of the filling and emptying of an oil storage tank (Shen et al., 1986), the simulation of a caisson-retained sand island in the Canadian Beaufort Sea (Kaliakin et al., 1990), and sundry simulations of true triaxial test results under drained conditions (Kaliakin and Pan, 2002; Kaliakin, 2005; Anantanasakul and Kaliakin, 2012; Jiang et al., 2013).

In the most recent study of the true triaxial response of clays, Kaliakin and Nieto-Leal (2012) investigated the existence of critical states under three-dimensional stress states. The results of this investigation indicated the possible need for a more refined failure criterion, as well as for more accurate stress–strain simulations under general states of stress.

This paper presents an improved shape hardening function that increases the accuracy of stress–strain simulations for moderately to heavily overconsolidated soils. This added accuracy is realized without any changes to the simple elliptical shape of the bounding surface (Kaliakin and Dafalias, 1989), and actually reduces the

* Corresponding author. Tel.: +1 (302) 831 2409.

E-mail addresses: andres.nieto@unimilitar.edu.co (A. Nieto-Leal), kaliakin@udel.edu (V.N. Kaliakin).

Peer review under responsibility of Institute of Rock and Soil Mechanics, Chinese Academy of Sciences.



number of parameters associated with the model by one. In order to better illustrate the effect of an improved shape hardening function on its predictive capabilities, in this paper the generalized bounding surface formulation (Kaliakin and Nieto-Leal, 2013) is specialized to a form suitable for isotropic cohesive soils.

2. General aspects of elastoplasticity

This section presents some general aspects related to a rate-independent elastoplastic formulation. These serve as a basis against which to contrast the bounding surface concept that is presented in the next section.

The material state is defined in terms of effective stresses σ'_{ij} (the external variables) and a set of internal variables q_n that embody the past loading history. In the subsequent development tensorial quantities are presented in indicial form with the indices obeying the summation convention over repeated indices. A single subscript for the plastic internal variables is not a tensorial index but merely identifies the plurality of these quantities.

Considering only infinitesimal displacements and displacement gradients, the usual additive decomposition of the total incremental strain tensor $d\varepsilon_{ij}$ into an elastic part $d\varepsilon_{ij}^e$ and a plastic part $d\varepsilon_{ij}^p$ is assumed, namely

$$d\varepsilon_{ij} = d\varepsilon_{ij}^e + d\varepsilon_{ij}^p \tag{1}$$

The incremental elastic constitutive relation is given by $d\varepsilon_{ij}^e = A_{ijkl}d\sigma'_{kl}$, where A_{ijkl} is a fourth-order tensor of compliance coefficients. Requirements of energy dissipation impose restrictions on these tensors such that the elastic strain and the stress can be derived from proper elastic potentials (Fung, 1965). However, for simplicity, the derivation from an elastic potential can be bypassed in favor of simpler hypoelastic relations.

The existence of a smooth, convex yield surface that separates the regions of purely elastic and plastic response in stress space is assumed. It is completely enclosed by a smooth loading surface that is not necessarily identical with the yield surface (Eisenberg and Phillips, 1971). The loading surface is analytically defined by

$$f^*(\sigma_{ij}, q_n) = 0 \tag{2}$$

Stress increments directed outward from the loading surface produce plastic deformations and are termed loading increments; those tangential to the surface and those directing inwards are termed neutral and unloading increments, respectively, and produce no plastic deformations.

A scalar loading index L is defined as follows:

$$L = \frac{1}{K_p}L_{ij}d\sigma'_{ij} = \frac{1}{K_p}\frac{\partial f^*}{\partial \sigma'_{ij}}d\sigma'_{ij} \tag{3}$$

where K_p is the scalar plastic modulus, and $L_{ij} = \partial f^* / \partial \sigma'_{ij}$ is the tensor acting in the direction normal to the loading surface. Loading, neutral loading and unloading occur when $L > 0$, $L = 0$ and $L < 0$, respectively.

Imposing the requirement of continuous material response with respect to a changing direction of $d\sigma$ across neutral loading (Dafalias and Popov, 1976), the incremental plastic constitutive relations are given by

$$\left. \begin{aligned} d\varepsilon_{ij}^p &= \langle L \rangle R_{ij} \\ dq_n &= \langle L \rangle r_n \end{aligned} \right\} \tag{4}$$

where the symbol “ $\langle \rangle$ ” denotes Macaulay brackets, which implies that $\langle L \rangle = L$ if $L > 0$ and $\langle L \rangle = 0$ if $L \leq 0$. The quantities R_{ij} and r_n

indicate the directions of $d\varepsilon_{ij}^p$ and dq_n , respectively, and are proper functions of the state. The R_{ij} is commonly assumed to be the gradient of a plastic potential Q , i.e. $R_{ij} = \partial Q / \partial \sigma'_{ij}$. Finally, the plastic modulus that appears in Eq. (3) is obtained from the consistency condition $df = 0$ which, in conjunction with Eqs. (2) and (3) and the second of Eq. (4), and assuming $L > 0$, gives

$$K_p = -\frac{\partial f^*}{\partial q_n}r_n \tag{5}$$

3. The bounding surface concept

In this section, some general aspects of the bounding surface concept associated with rate-independent plasticity are presented in order to facilitate the subsequent discussion of the improved shape hardening function. Further details pertaining to the bounding surface concept were given in Dafalias (1986b).

The bounding surface concept was motivated by the observation that any stress–strain curve for monotonic loading, or for monotonic loading followed by reverse loading, eventually converges to certain well-defined “bounds” in the stress–strain space (Dafalias and Popov, 1975; Krieg, 1975). These bounds cannot be crossed but may change position in the process of loading. In addition, the rate of convergence, expressed by means of the plastic modulus, depends upon the “norm” or “distance” (in a proper metric space) between the current state and a corresponding “bounding” state.

The evolution of the bounding state and the interrelation with the actual state by means of the distance offers a general framework for the development of realistic elastoplastic constitutive models. A microscopic interpretation of the bounding state can be made by associating it with the packing history incurred by soil particles (Mröz et al., 1978). However, because in the process of deformation the bounding state evolves, it is not identical to a limit state for metals, or to a critical state (where unrestricted flow occurs) for soils.

For the development of constitutive models, the simplest way to describe the bounding state is by means of the concept of a bounding surface in stress space (Dafalias, 1981). In models appropriate for soils, the bounding surface always encloses the origin and is origin-convex, i.e. any radius emanating from the origin intersects the surface at only one point (Fig. 1).

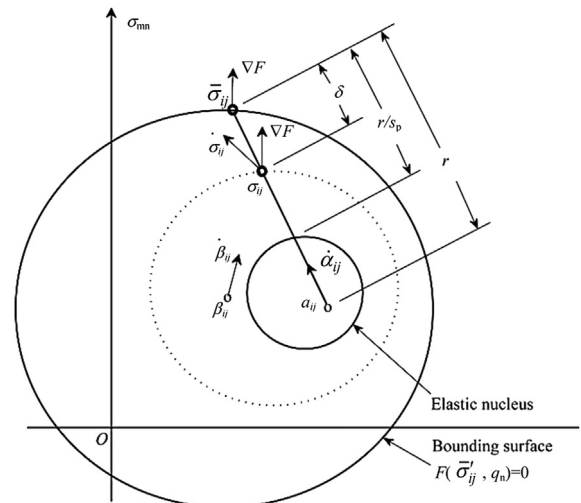


Fig. 1. Schematic illustration of the bounding surface and radial mapping rule in multiaxial space.

The essence of the bounding surface concept is the hypothesis that plastic deformations can occur for stress states either within or on the bounding surface. Thus, unlike classical yield surface elastoplasticity, the plastic states are not restricted only to those lying on a surface. This fact has proven to be a great advantage of the bounding surface concept.

If the material state is defined in terms of σ'_{ij} and proper q_n , then the bounding surface in stress space is defined analytically by

$$F(\bar{\sigma}'_{ij}, q_n) = 0 \quad (6)$$

where a bar over stress quantities indicates an “image” point on the bounding surface. The actual stress point σ'_{ij} lies always within or on the surface. To each σ'_{ij} a unique “image” stress point $\bar{\sigma}'_{ij}$ is assigned by a properly defined “mapping” rule that becomes the identity mapping if σ'_{ij} is on the surface.

In an effort to simplify earlier formulations, Dafalias (1979a) introduced a very simple “radial mapping” rule that does not require an explicit definition of a yield surface. A similar mapping rule had been introduced earlier by Hashiguchi and Ueno (1977). The radial mapping rule combines simplicity and ease of numerical implementation, and has been shown to accurately predict the rate-independent elastoplastic behavior of cohesive soils (Dafalias and Herrmann, 1980, 1982a,b; Dafalias et al., 1982; Dafalias and Herrmann, 1986). For these reasons, the radial mapping rule is used in the present development.

In the resulting bounding surface model as shown schematically in Fig. 1, it is assumed that the projection center α_{ij} lies always within a convex bounding surface and never crosses it. The α_{ij} may be thought of as a second back-stress in addition to the geometric center β_{ij} of the bounding surface. The α_{ij} evolves according to a proper rate equation, and is one of the internal variables. It does not, however, enter into the analytical expression for the bounding surface. Using the α_{ij} as the projection center, the “image” stress is obtained by the radial projection of the actual stress onto the surface according to

$$\bar{\sigma}'_{ij} = b(\sigma'_{ij} - \alpha_{ij}) + \alpha_{ij} \quad (7)$$

where the dimensionless parameter $1 \leq b \leq \infty$ can be determined in terms of the material state by substituting $\bar{\sigma}'_{ij}$ from Eq. (7) into an explicit form of Eq. (6), and solving the resulting expression for b .

A consequence of assuming the radial mapping rule is that a surface homologous to the bounding surface with respect to the projection center α_{ij} and passing through the actual stress point (σ'_{ij}) is indirectly defined. This surface, shown dashed in Fig. 1, determines all the paths of neutral loading emanating from σ'_{ij} , and defines a quasi-elastic domain. However, since the stress point may first move elastically inwards and then cause plastic loading before again reaching the surface, this surface is not a yield surface. It is closer to the concept of a loading surface (Eisenberg and Phillips, 1971), but is not entirely equivalent to it since no consistency condition is required.

The bounding surface is instrumental in defining the direction of plastic loading—unloading L_{ij} (Eq. (3)) and the plastic modulus K_p (Eq. (5)). The expression for L_{ij} at σ'_{ij} is defined as the gradient of F at the “image” point, namely

$$L_{ij} = \frac{\partial F}{\partial \bar{\sigma}'_{ij}} \quad (8)$$

For any stress increment $d\sigma'_{ij}$ causing plastic loading, a corresponding image stress increment $d\bar{\sigma}'_{ij}$ occurs as a result of the hardening of the bounding surface by means of the internal

variable q_n . The following relations are thus required to complete the general bounding surface formulation:

A scalar loading index (Eq. (3)) is defined in terms of Eq. (8), the stress increments $d\sigma'_{ij}$, $d\bar{\sigma}'_{ij}$, the plastic modulus K_p (associated with σ'_{ij}) and a “bounding” plastic modulus \bar{K}_p (associated with $\bar{\sigma}'_{ij}$), i.e.

$$L = \frac{1}{K_p} \frac{\partial F}{\partial \sigma'_{ij}} d\sigma'_{ij} = \frac{1}{\bar{K}_p} \frac{\partial F}{\partial \bar{\sigma}'_{ij}} d\bar{\sigma}'_{ij} \quad (9)$$

A bounding plastic modulus \bar{K}_p is obtained from the consistency condition $dF = 0$. Using Eqs. (4) and (6) along with the last term of Eq. (9) gives

$$\bar{K}_p = -\frac{\partial F}{\partial q_n} r_n \quad (10)$$

A state-dependent relation between K_p and \bar{K}_p is established as a function of the Euclidean distance δ between the current stress state and its “image” stress (Fig. 1), viz.

$$K_p = \bar{K}_p + \hat{H}(\sigma'_{ij}, q_n) \frac{\delta}{r - \delta} \quad (11)$$

where r represents a properly chosen and possibly varying reference stress or distance, such that $r - \delta \geq 0$. The quantity \hat{H} denotes a proper scalar shape hardening function of the state. The exact definition of \hat{H} requires the identification and experimental determination of certain material parameters (to be discussed in a subsequent section).

Eq. (11), which is by no means unique, embodies the meaning of the bounding surface concept. If $\delta < r$ and \hat{H} is not approaching infinity, the concept allows for plastic deformations to occur for points either within or on the surface at a progressive pace that depends upon δ . The closer to the bounding surface is the actual stress point (σ'_{ij}), the smaller is K_p (it approaches the corresponding \bar{K}_p), and the greater is the plastic strain increment for a given stress increment. The σ'_{ij} may eventually reach the bounding surface in the course of plastic loading; it remains on the surface (i.e. $\delta = 0$) if loading continues, and detaches from the surface and moves inwards upon unloading. Thus, for states within the bounding surface (i.e. for $\delta > 0$), the function \hat{H} and its associated parameters are intimately related to the material response. As such, they constitute important “new” elements of the present formulation with regard to ones based on classical yield surface elastoplasticity.

4. Formulation for isotropic cohesive soils

The elastoplastic bounding surface formulation developed to this point is quite general and it is only the concept of effective stress that makes it appropriate for soils as well. Any type of material symmetries can now be incorporated into the formulation by properly defining the elastic moduli and rendering the bounding surface, a function of proper invariant quantities of the effective stress and the internal variables. In this section the generalized bounding surface formulation (Kaliakin and Nieto-Leal, 2013) is specialized for isotropic cohesive soils.

4.1. Stress invariants

Invariance requirements under superposed rigid body rotation require that the bounding surface be a function of the direct isotropic invariants of $\bar{\sigma}'_{ij}$ and q_n . Along the lines of the rate-independent formulation presented by Dafalias and Herrmann (1982b), the dependence of the surface on σ'_{ij} is expressed in terms of the first effective stress invariant I_1 , the square root of the

second deviatoric stress invariant J , and the Lode angle θ (Zienkiewicz and Pande, 1977), given by

$$I_1 = \sigma'_{ij} \delta_{ij} = \sigma'_{kk} \tag{12}$$

$$J = \sqrt{\frac{1}{2} s_{ij} s_{ij}} \tag{13}$$

$$\theta = \frac{1}{3} \sin^{-1} \left[\frac{3\sqrt{3}}{2} \left(\frac{S}{J} \right)^3 \right]; \quad -\frac{\pi}{6} \leq \theta \leq \frac{\pi}{6} \tag{14}$$

where $S = (s_{ij} s_{jk} s_{ki} / 3)^{1/3}$ is the third root of the third deviatoric stress invariant.

4.2. Hardening of the surface

The bounding surface is assumed to undergo isotropic hardening along the hydrostatic (I_1) axis. The hardening is controlled by a single scalar internal variable that measures the plastic change in volumetric strain $d\varepsilon_{kk}^p$. Denoting the total void ratio by e and by e^e and e^p (its elastic and plastic parts, respectively), it follows that $e = e^e + e^p$. The increments of ε_{kk}^p and e^p are then related according to

$$de^p = -(1 + e_{in}) d\varepsilon_{kk}^p = -(1 + e_{in}) \langle L \rangle R_{kk} \tag{15}$$

where e_{in} represents the initial total void ratio corresponding to the reference configuration with respect to which engineering strains are measured. For natural strains, e_{in} represents the current total void ratio.

It is convenient to relate the evolution of the bounding surface to the inelastic void ratio through the value of I_0 , which represents the point of intersection of the bounding surface with the positive part of the I_1 -axis in invariant stress space (Fig. 2), and measures the amount of preconsolidation of the soil. For an isotropic soil consolidated isotropically (i.e. along the I_1 -axis), only volumetric strains are generated. This fact, in conjunction with Eq. (15), implies that I_0 must depend only on e^p . Therefore, an expression for $dI_0 = de^p$, necessary for the analytical description of the hardening behavior, is now sought.

Although the hardening of the bounding surface can be described analytically in a number of ways, past practice has employed aspects of critical state soil mechanics (Schofield and Wroth, 1968). Using such an approach leads to the following expression (Dafalias and Herrmann, 1986):

$$\frac{dI_0}{de^p} = -\frac{\langle I_0 - I_L \rangle + I_L}{\lambda - \kappa} \tag{16}$$

where the critical state parameters λ and κ denote the slopes of the isotropic consolidation and swell/recompression lines, respectively, in a plot of void ratio versus the natural logarithm of I_1 , and I_L is a nonzero limit value of I_1 such that for $I_1 < I_L$ the relation between I_1 and the elastic part of the void ratio (e^e) changes continuously from logarithmic to linear (Dafalias and Herrmann, 1986). In this manner, the singularity of the elastic stiffness near $I_1 = 0$ (resulting from excessive material softening) is removed. It is important to note that I_L is *not* a model parameter; its value is typically taken equal to one-third of the atmospheric pressure P_a .

The elastic response is assumed to be isotropic. It is further assumed to be independent of the rate of loading, and to be unaltered by inelastic deformation. The consequence of adopting aspects of critical state soil mechanics is that the elastic bulk modulus becomes a function of I_1 according to

$$K = \frac{1 + e_{in}}{3\kappa} (\langle I_1 - I_L \rangle + I_L) \tag{17}$$

The elastic shear modulus G is either defined independently, or is computed from K and a specified value of Poisson's ratio (ν). Based upon the above discussion, and recalling Eq. (6), the bounding surface is defined analytically by

$$F(\bar{I}_1, \bar{J}, \bar{\theta}, I_0) = 0 \tag{18}$$

Eq. (18) can assume many specific forms provided certain conditions regarding the chosen shape are satisfied. A specific analytical expression for the bounding surface is presented in Section 6.

4.3. Specialization of the formulation

The radial mapping rule given by Eq. (7) is specialized by explicitly defining the projection center α_{ij} , as well as its evolution. Since isotropy is assumed, the projection center must be an isotropic tensor with a principal value $I_1 = I_c$ on the I_1 -axis in invariant stress space, i.e. $\alpha_{ij} = 1/3 \delta_{ij} I_c$ (Dafalias and Herrmann, 1986). In past applications of the bounding surface plasticity model for cohesive soils, the projection center was fixed at the stress origin ($I_1 = J = 0$). Motivated by the less-than-satisfactory analytical predictions for samples having a large initial degree of overconsolidation, Dafalias (1982a) proposed a generalization of earlier forms of Eq. (7) that defines an image stress state given by

$$\bar{I}_1 = b(I_1 - I_c) + I_c = b(I_1 - C I_0) + C I_0 \tag{19}$$

$$\left. \begin{aligned} \bar{s}_{ij} &= b s_{ij} \\ \bar{J} &= b J \\ \bar{S} &= b S \end{aligned} \right\} \tag{20}$$

where C is a dimensionless model parameter ($0 \leq C < 1$).

This modification introduces the possibility of using a projection center $I_c = C I_0$ in stress space different from the origin (Fig. 2). This form of the radial mapping rule introduces a kind of "hydrostatic back-stress", I_c , and allows for the prediction of immediate negative (dilatational) pore pressure development for heavily overconsolidated samples sheared under undrained loading conditions. With the projection center at the origin ($C = 0$), the older formulation is retrieved, with initially positive pore pressures always being predicted, even for highly overconsolidation samples. As a consequence of the last two of Eq. (20), it follows that $\bar{S}/\bar{J} = S/J$

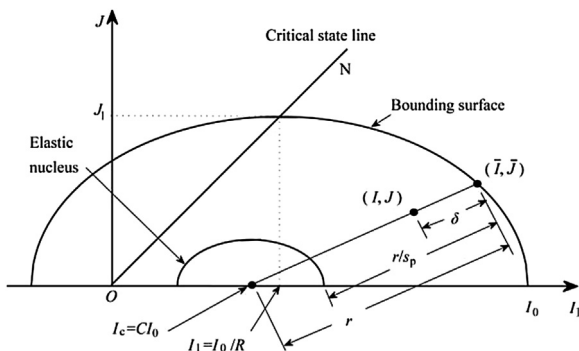


Fig. 2. Schematic illustration of elliptical bounding surface and radial mapping rule in stress invariants space.

means that the actual and image stress points are characterized by the same Lode angle, that is, $\bar{\theta} = \theta$.

The generalized bounding surface model is further specialized by assuming an associative flow rule, that is, $R_{ij} = L_{ij} = \partial F / \partial \bar{\sigma}_{ij}$. Expanding R_{ij} in terms of derivatives of F with respect to I_1, J and θ gives $R_{kk} = 3(\partial F / \partial I_1)$.

The general expression for the “bounding” plastic modulus \bar{K}_p is obtained from the consistency condition $dF(\bar{I}_1, \bar{J}, \bar{\theta}, I_0) = 0$. Using Eq. (15) along with the above expression for R_{kk} gives

$$\bar{K}_p = -\frac{3(1 + e_{in})}{\lambda - \kappa} ((I_0 - I_L) + I_L) \frac{\partial F}{\partial I_1} \frac{\partial F}{\partial I_0} \quad (21)$$

where Eq. (16) was used.

5. The failure criterion

For a specific value of the Lode angle θ , the failure surface reduces to a straight line that is assumed to coincide with the critical state line (Schofield and Wroth, 1968). In I_1 - J space, the slope of the critical state line is denoted by N . The variation of N with θ is described as follows:

$$\left. \begin{aligned} N(\theta) &= g(\theta, k) N_c \\ k &= N_e / N_c \end{aligned} \right\} \quad (22)$$

The $N_e = N(-\pi/6)$ and $N_c = N(\pi/6)$ are the values of $N(\theta)$ associated with axisymmetric triaxial extension and compression, respectively.

The dimensionless function $g(\theta, k)$ must take on the values $g(-\pi/6, k) = k$ and $g(\pi/6, k) = 1$. A simple form of this function, attributed to Gudehus (1973) and Zienkiewicz and Pande (1977) and then used (Dafalias and Herrmann, 1982b, 1986; Dafalias et al., 1982) in conjunction with bounding surface models for clays, is

$$g(\theta, k) = \frac{2k}{1 + k - (1 - k)\sin(3\theta)} \quad (23)$$

Although the accuracy of Eq. (23) for representing the variation of the failure criterion with θ for three-dimensional stress states has recently been questioned (Kaliakin and Nieto-Leal, 2012), it is nonetheless used herein.

6. Specific form of the bounding surface

The analytical definition of the bounding surface, described in general by Eq. (18), is assumed to be an ellipse (Kaliakin and Dafalias, 1989):

$$F = (\bar{I}_1 - I_0) \left(\bar{I}_1 + \frac{R-2}{R} I_0 \right) + (R-1)^2 \left[\frac{\bar{J}}{N(\theta)} \right]^2 = 0 \quad (24)$$

where $R \geq 2.0$ is a dimensionless model parameter that controls the shape of the elliptic surface. In particular, larger values of R imply a “flatter” surface. Fig. 2 shows a section of this surface for a given value of θ , along with its associated parameters C and R . The failure surface $N(\theta)$ is given by Eq. (22).

7. The shape hardening function

The hardening function \hat{H} defines the shape of the response curves during inelastic hardening (or softening) for points within the bounding surface (i.e. for $\delta > 0$). It relates the plastic modulus K_p to its “bounding” value \bar{K}_p in the following general manner:

$$K_p = \bar{K}_p + \hat{H}(\sigma_{ij}, q_n) \hat{f}(\delta) \quad (25)$$

Eq. (25) is seen to be a generalization of Eq. (11), with \bar{K}_p given by Eq. (21). Eqs. (10) and (25) differentiate the bounding surface formulation from standard elastoplasticity models. In these equations, the plastic moduli K_p and \bar{K}_p both have units of stress cubed. Noting that $\hat{f}(\delta)$ is dimensionless, it follows that \hat{H} must also have units of stress cubed. Since \hat{H} is the focus of this paper, it is necessary to review some specific forms of this function that have been used in the past.

7.1. Composite form of the bounding surface

Dafalias and Herrmann (1986) used the following functional form of \hat{H} in conjunction with the “composite” form of the bounding surface consisting of two ellipses and a hyperbola:

$$\hat{H} = \frac{1 + e_{in}}{\lambda - \kappa} P_a \left[9(F_{I_1})^2 + \frac{1}{3}(F_J)^2 \right] \left[h(\theta)z^{0.02} + h_0(1 - z^{0.02}) \right] f \quad (26)$$

where $z = J/J_1 = JR/NI_0$ is a dimensionless variable, and f is equal to unity. The term $1 + e_{in}$ is included in Eq. (26) because of its presence in the expression for \bar{K}_p in Eq. (21). The quantity P_a is the atmospheric pressure; it is included to give H the proper units of stress cubed. The quantity $(\lambda - \kappa)$ is introduced into Eq. (26) only for similarity to the aforementioned Eq. (21) for \bar{K}_p . The quantity h_0 represents the hardening parameter for states in the immediate vicinity of the I_1 -axis (i.e. for $z \approx 0$).

The first bracketed quantity in Eq. (26) was required to preserve continuity of the stress rate–strain rate relation in the composite form of the bounding surface (Dafalias and Herrmann, 1986). Subsequent experience has shown that even for the simpler single ellipse version of the surface (Kaliakin and Dafalias, 1989) that is further discussed in the following section, this quantity should be retained in the functional form for \hat{H} .

The dimensionless quantity $h(\theta)$ defines the degree of hardening for points within the bounding surface, except those within the immediate vicinity of the I_1 -axis where $z \rightarrow 0$. Of all the hardening quantities, $h(\theta)$ has the most fundamental and significant role. It is a function of the Lode angle θ and varies in magnitude from a value of $h_c = h(\pi/6)$ (corresponding to a state of triaxial compression) to a value of $h_e = h(-\pi/6)$ (corresponding to a state of triaxial extension). More precisely, this interpolation is given by

$$h(\theta) = \frac{2\mu}{1 + \mu - (1 - \mu)\sin(3\theta)} h_c = g(\theta, \mu) h_c \quad (27)$$

where $\mu = h_e/h_c$.

The quantity h_0 is included in the formulation to ensure continuity when the stress point crosses the I_1 -axis, thereby improving numerical behavior in this region. For simulations involving both triaxial compression and extension, it is very important to properly compute h_0 so as to ensure a relatively smooth transition between h_c and h_e . Since it is typically set equal to the average of h_c and h_e , h_0 does not explicitly enter into the calibration process for the model parameters.

In the second bracketed quantity in Eq. (26), the term $z^{0.02}$ may be thought of as a weighting factor with respect to $h(\theta)$ and h_0 . The small exponent (0.02) on z renders the quantity $z^{0.02} \approx 1$, even for small nonzero values of z . Thus, for stress states off the I_1 -axis (e.g. for $J \neq 0$), $h(\theta)$ will be the predominant term in the second bracketed quantity. For hydrostatic states of stress (i.e. $J = 0$) this quantity will be equal to h_0 .

Finally, Dafalias and Herrmann (1986) assumed the following expression for $\hat{f}(\delta)$ appearing in Eq. (25):

$$\hat{f}(\delta) = \frac{\delta}{\langle r - s_p \delta \rangle} = \left\langle \frac{b}{b-1} - s_p \right\rangle^{-1} \quad (28)$$

where s_p ($s_p \geq 1$) is a model parameter that defines the size of the “elastic nucleus” (Fig. 2), and b is as defined in Eq. (7). If $s_p = 1$, the elastic nucleus reduces to a point, resulting in elastoplastic response being predicted within the entire bounding surface.

7.2. Single ellipse form of the bounding surface

In an effort to simplify the aforementioned composite form of the bounding surface, a simpler formulation for isotropic cohesive soils consisting of a single ellipse was developed (Kaliakin and Dafalias, 1989). The associated functional form of \hat{H} is again given by Eq. (26). Although the adoption of a single ellipse simplifies the explicit definition of the bounding surface, it requires the modification of previous functional forms of \hat{H} . More precisely, if a single ellipse is used instead of a hyperbola associated with the composite form of the surface (which is closer to the critical state line), undesirably high levels of J will be attained at moderate to large overconsolidation ratios (OCRs). To prevent this from occurring, the following functional form of f (in Eq. (26)) was added to the expression for \hat{H} (Kaliakin and Dafalias, 1989):

$$f = \frac{1}{2} \left[a + \text{sign}(n'_p) \left(|n'_p| \right)^{1/w} \right] \quad (29)$$

where a and w are dimensionless model parameters. The quantity n'_p is the component in the p' -direction ($p' = I_1/3$) of the unit outward normal to the bounding surface in triaxial stress space; as such, it is a dimensionless quantity.

Since the use of a single ellipse alleviates the issue of maintaining continuity of the response as the material point proceeds from one portion of the surface to the other, the first bracketed quantity in Eq. (26) could be replaced by P_a^2 , as was done by Manzari and Nour (1997). However, experience shows that the resulting simulations for overconsolidated soils (i.e. stress states within the bounding surface) are not as good as when this quantity is included. This is explained by the fact that both F_{i_1} and F_j vary during the course of a typical stress path, whereas P_a is a constant.

7.3. Improved shape hardening function

In order to further improve the predictive capabilities of the isotropic bounding surface model employing a single ellipse, Eq. (26) was modified by replacing Eq. (29) with the following expression:

$$f = \frac{1}{2} \left[a + \text{sign}(n'_p) \left(|n'_p| \right)^{1/5} \right] \left(\frac{I_1}{I_0} \right) \quad (30)$$

Comparing Eqs. (29) and (30), it is evident that the model parameter w is no longer present in the latter. Finally, the term (I_1/I_0) has been added to Eq. (30) so as to better account for the overconsolidation ratio in the functional form of \hat{H} .

To facilitate the discussion of f , the following triaxial space parameter is defined: $\eta = q/p'$. The actual state need not, however, be triaxial. The quantity n_p thus ranges in value from +1 (corresponding to $\eta = 0$ and $p' > 0$) to -1 (for $\eta = 0$ and $p' < 0$). When the “image” stress is at the intersection of the bounding surface with the critical state line (i.e. when $\eta = M$), $n_p = 0$.

The parameter a must be greater than unity. Letting a take on a “typical” value of 2.0, f will vary between a value of 1.50 (corresponding to $\eta = 0$ and $n_p = +1$), through a value of 1.0 (corresponding to $\eta = M$ and $n_p = 0$), to a value of 0.50 (corresponding to $\eta = 0$ and $n_p = -1$) times (I_1/I_0) . It is worthwhile to observe that the largest variation of f (from 1.50 to 0.50) occurs as η goes through the value of M , which is a desirable feature. In this manner, the predicted material response at large OCRs will be “softer” when $\eta > M$, thus preventing the attainment of high levels of J . Through the presence of n_p , the quantity f , and consequently \hat{H} and K_p , are essentially made proper functions of η and the degree of overconsolidation.

Besides reducing the number of model parameters by one, the new expression for f better incorporates the effect of overconsolidation into the expression for \hat{H} . The predictive capabilities of the model employing this new form of \hat{H} are now assessed.

8. Assessment of predictive capabilities

In this section, the predictive capabilities of the isotropic bounding surface model consisting of a single ellipse with the improved \hat{H} given by Eqs. (26) and (30) are assessed. This assessment is realized by comparing this form of the model to experimental results, and to simulations obtained using \hat{H} given by Eq. (26) with f either equal to unity (and thus associated with the composite form of the bounding surface), or equal to the expression given in Eq. (29) (and thus associated with the original form of the bounding surface consisting of a single ellipse).

The following model parameters are associated with both versions of the model: the critical state parameters (λ , κ , M_c and M_e), the elastic parameters (shear modulus G or Poisson’s ratio ν), the bounding surface configuration parameter (R), the projection center parameter (C), the elastic nucleus parameter (s_p), and the shape hardening parameters (h_c and h_e). In addition, the composite form of the bounding surface model requires values for the parameter R_e (that defines the shape of the first ellipse in extension), the parameters A_c and A_e (associated with the hyperbola, in triaxial compression and extension, respectively), as well as the parameter T (that defines the second, or tension ellipse). For \hat{H} with f given by Eq. (29), the parameters a and w must also be included. Finally, the improved \hat{H} with f given by Eq. (30) only requires the single additional parameter a .

8.1. Simulation of undrained shearing of a kaolin mixture

The soil used in the first set of simulations is a laboratory prepared mixture of two commercial grades of kaolin (liquid limit = 37 and plasticity index = 8). Shen et al. (1986) used this soil in centrifuge experiments that served to validate the predictive capabilities of the bounding surface model for isotropically consolidated cohesive soils. For this purpose, the kaolin mixture was originally characterized using the composite form of the bounding surface consisting of two ellipses and one hyperbola. It is thus of interest to compare this previous simulation with similar ones obtained using the single ellipse version of the model.

In addition to standard consolidation tests, a series of six isotropically consolidated undrained tests were performed using an axisymmetric triaxial device. Three tests were performed in compression and three in extension. The OCRs for each group of tests were equal to 1.0, 2.0 and 6.0.

Values for the traditional critical state parameters were taken from Shen et al. (1986). In particular, $\lambda = 0.0745$, $\kappa = 0.0105$, $M_c = 1.35$, $M_e = 0.90$, and $\nu = 0.22$. For the version of the model employing a composite form of the bounding surface, the values of the parameters $R_c = 3.05$ and $R_e = 1.71$ were determined by

matching the shape of the undrained stress paths in triaxial compression and extension, respectively. The value of the projection center parameter $C = 0.485$ was determined from the shapes of all six undrained stress paths. The values of the bounding surface parameters that determine the size of the hyperbola ($A_c = 0.175$ and $A_e = 0.149$), as well as the hardening parameters $h_c = 11.0$ and $h_e = 9.63$ were determined by matching the results for OCR equal to 6.0 in triaxial compression and extension. Using the above parameter values in conjunction with the composite form of the bounding surface, the undrained simulations shown in Fig. 3a–c were generated. From these figures, it is evident that the simulations obtained using the composite form of the bounding surface are in very good agreement with the experimental results.

The simulations were next repeated using the single ellipse version of the model. The values of the parameters $\lambda, \kappa, M_c, M_e$ and ν were unchanged from those used in conjunction with the composite form of the surface. The single value of the bounding surface parameter R now applies to both triaxial compression and extension. As such, some compromise in the simulative capabilities is expected. After some trial analyses, it was determined that letting $R = 3.05$ gave the best simulations of undrained results. Since it is largely determined by the shapes of the undrained stress paths (and applies for both triaxial compression and extension), the value of the projection center parameter C was unchanged from that used in conjunction with the composite form of the bounding surface. The values for the hardening parameters h_c and h_e were likewise unchanged from those in the composite form of the bounding surface. The values of the parameters A_c, A_e and T no longer apply to the single ellipse version of the model. Instead the hardening parameters a and w , that appear in Eq. (29), must be used. Based on past experience, values of 1.20 and 5.0 were used for a and w , respectively. Using these parameter values, undrained simulations similar to those shown in Fig. 3a–c were generated and shall be assessed below.

Finally, the simulations were again performed using the single ellipse version of the model, only employing a modified shape hardening function of Eq. (26) with f given by Eq. (30). The values of the parameters $\lambda, \kappa, M_c, M_e, \nu, R, C, s_p, h_c$ and h_e were unchanged from those used in conjunction with the previous simulations employing the single ellipse form of the bounding surface. The parameter a now is equal to 7.0, and the parameter w is no longer required. Using these parameter values, undrained simulations similar to those shown in Fig. 3a–c were generated. To better understand the effect of using the improved shape hardening function on the simulations, the material response in triaxial compression is considered. In the legends of Fig. 4a–c, the designation “($f = 1.0$)” refers to the composite form of the bounding surface, and “(f from Eq. (29))” and “(f from Eq. (30))” refer to the single ellipse version of the bounding surface with f given by Eqs. (29) and (30), respectively. From Fig. 4a–c, it is evident that the improved shape hardening function with f given by Eq. (30) gives results that are closer to the experimental ones than those obtained using either the composite form of the bounding surface (i.e. for $f = 1.0$), or those obtained using Eq. (29). In short, even though the improved \hat{H} requires one less model parameter as compared to the function that uses Eq. (29), it nonetheless produces more accurate simulations.

8.2. Simulation of lower Cromer till response

The single ellipse version of the isotropic bounding surface model was also used to simulate the response of isotropically consolidated lower Cromer till (LCT), based on the work of Gens (1982). LCT is classified as a low-plasticity sandy silty-clay (liquid limit = 25 and plasticity index = 13), with the main clay minerals being calcite and illite. The tests on LCT were all performed on

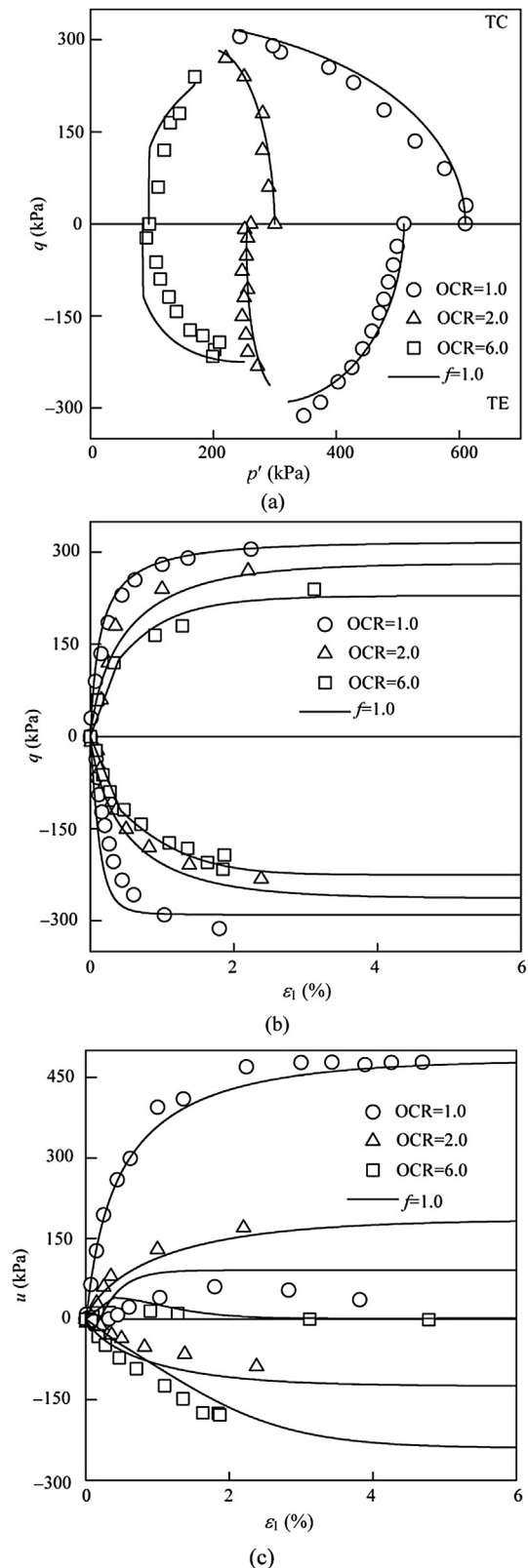


Fig. 3. Simulations for triaxial compression (TC) and triaxial extension (TE) for the UCD kaolin mixture obtained using the “composite” form of the bounding surface. u is the pore water pressure.

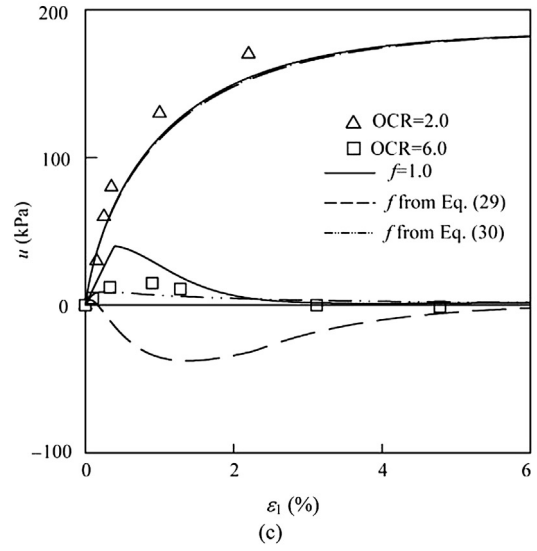
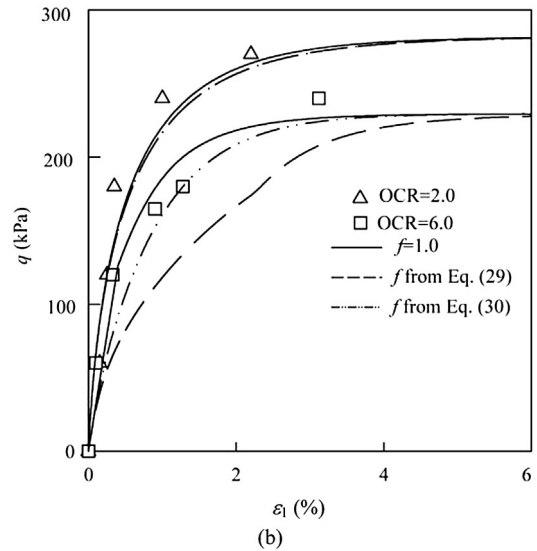
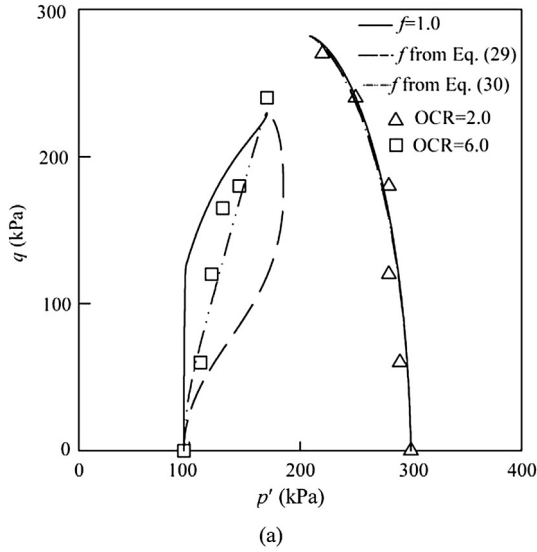


Fig. 4. Comparison of model simulations in triaxial compression for the UCD kaolin mixture with OCR = 2.0 and OCR = 6.0 obtained using the “composite” form of the bounding surface ($f = 1.0$), f given by Eq. (29), and f given by Eq. (30), respectively.

samples consolidated from a slurry with an initial water content of 31%. Although the bounding surface model has traditionally been applied to rather soft clays with larger liquid limits and plasticity indices, the choice of LCT is motivated by its use in the verification of other clay models (Dafalias et al., 2006).

Values for the traditional critical state parameters were computed from the data of Gens (1982). In particular, $\lambda = 0.066$, $\kappa = 0.0077$, $M_c = 1.18$, $M_e = 0.86$, and $\nu = 0.20$. A value of 2.30 for the parameter R defining the shape of the elliptical bounding surface was determined from the experimental undrained stress paths for normally consolidated samples in triaxial compression and extension. A value of 0.52 for the projection center parameter C was determined by the shapes of the undrained stress paths for lightly overconsolidated samples. The rather “stiff” nature of these undrained stress paths required a value of 2.0 for the elastic nucleus parameter s_p . Finally, the values of $h_c = 1.0$ and $h_e = 5.0$ were determined by matching the stress-strain response of overconsolidated samples. For the version of the model with f given by Eq. (29), values of $a = 6.0$ and $w = 5.0$ were determined so as to best match the results of moderately and heavily overconsolidated samples. For the version of the model using the improved \hat{H} with

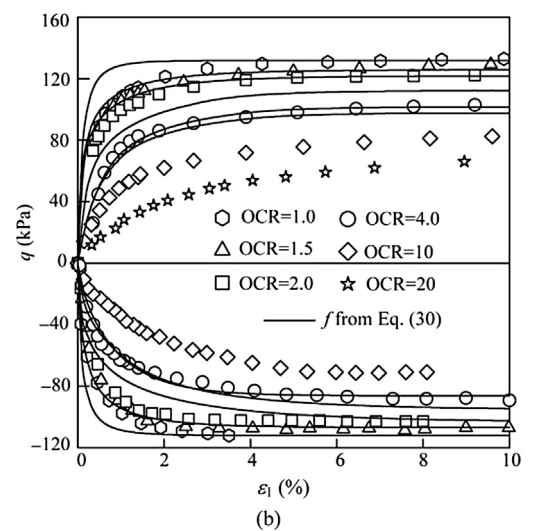
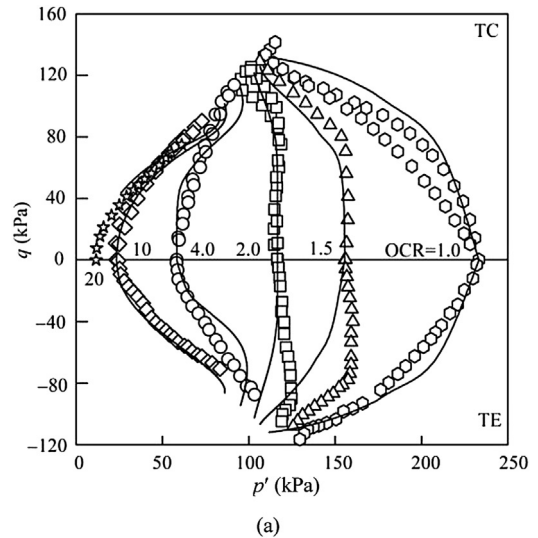


Fig. 5. Simulations for triaxial compression (TC) and triaxial extension (TE) for LCT obtained using the single ellipse form of the bounding surface with f given by Eq. (30).

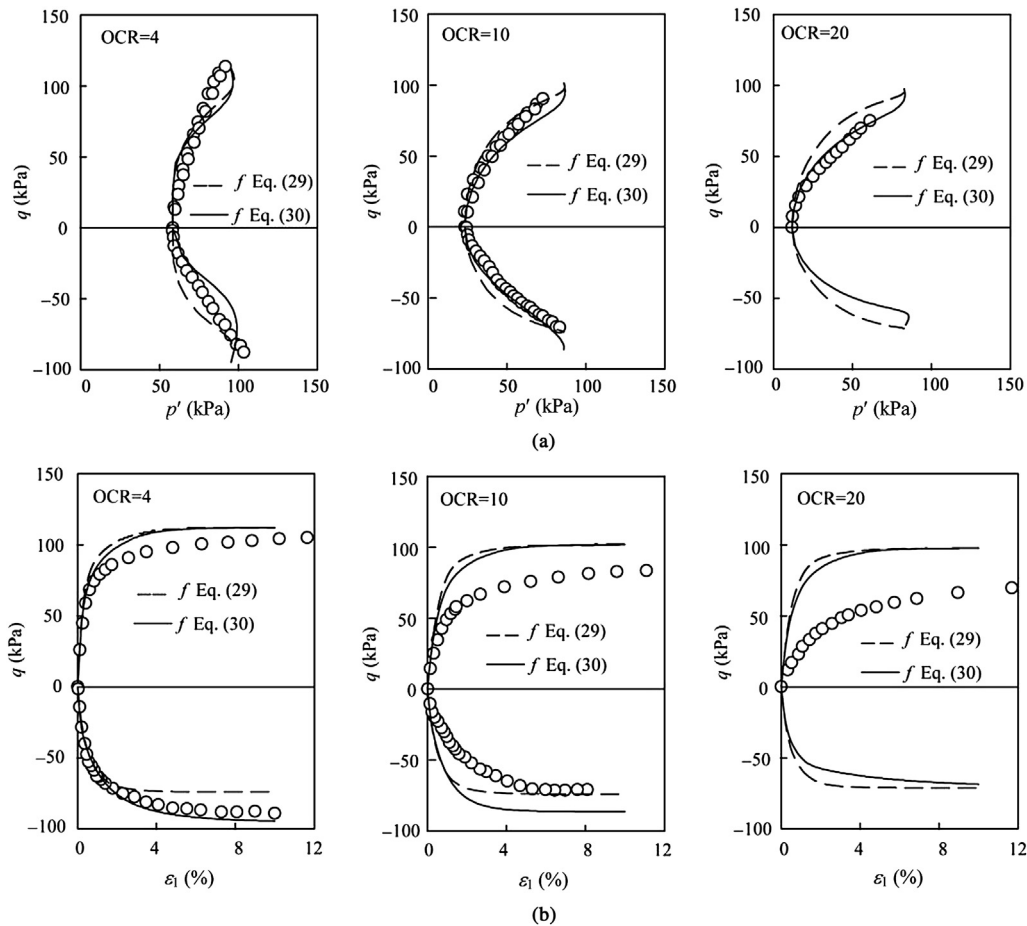


Fig. 6. Comparison of model simulations for LCT with OCR = 4, 10 and 20 obtained using the single ellipse form of the bounding surface with f given by Eqs. (29) and (30).

given by Eq. (30) the value of h_c needed to be increased to 5.0, and a value of a equal to 2.50 was found to give the best match with experimental results. Fig. 5a and b compares the numerical and experimental undrained stress paths and stress-strain response, respectively, using the improved version.

As noted in the previous simulations of the kaolin mixture, the improved shape hardening function primarily affects the material response at high OCRs. Thus, in order to better investigate the effect using the improved shape hardening function, Fig. 6a compares the undrained stress paths for OCRs equal to 4, 10 and 20. As evident from this figure, the improved \hat{H} slightly improves the simulated undrained stress paths at higher OCRs. Fig. 6b compares the deviator stress-axial strain response for the same OCRs. It is evident that the improved \hat{H} gives somewhat more accurate stress-strain paths than for the version of the function that uses Eq. (29). It is important to note that this is achieved with one less model parameter.

9. Conclusion

The use of an improved shape hardening function has been shown to accurately simulate the stress-strain response for over-consolidated cohesive soils. This has been demonstrated under both axisymmetric triaxial compression and extension states of stress. The use of an improved shape hardening function is a far simpler way in which to improve the simulated response of cohesive soils as compared to choosing a different, and typically more complex, analytical expression for the bounding surface.

Furthermore, this function actually reduces by one the number of parameters associated with the model.

Conflict of interest

We wish to confirm that there are no known conflicts of interest associated with this publication and there has been no significant financial support for this work that could have influenced its outcome.

Acknowledgment

The first author's graduate studies are supported by the Fulbright Colombia-Colciencias Scholarship and Universidad Militar Nueva Granada. This support is gratefully acknowledged.

References

- Anandarajah A, Dafalias YF. Bounding surface plasticity iii: application to anisotropic cohesive soils. *Journal of Engineering Mechanics, ASCE* 1986;112(12): 1292–318.
- Anantanasakul P, Kaliakin VN. Simulations of 3-D drained behavior of normally consolidated clay using elastoplastic models. In: *GeoCongress*, vol. GSP 225. ASCE; 2012. pp. 1076–85.
- Dafalias YF. A bounding surface plasticity model. In: *Proceedings of the Seventh Canadian Congress of Applied Mechanics*. Sherbrooke, Canada; 1979. pp. 89–90.
- Dafalias YF. A model for soil behavior under monotonic and cyclic loading conditions. In: *Transactions of the Fifth International Conference on SMIRT*, vol. 1. Berlin, Germany; 1979b. (Division K1/8): 1–9.

- Dafalias YF. The concept and application of the bounding surface in plasticity theory. In: IUTAM symposium on physical non-linearities in structural analysis. Senlis, France: Springer Berlin Heidelberg; 1981. pp. 56–63.
- Dafalias YF. Bounding surface elastoplasticity viscoplasticity for particulate cohesive media. In: IUTAM symposium on deformation and failure of granular materials. Rotterdam: A.A. Balkema; 1982a. pp. 97–107.
- Dafalias YF. On rate dependence and anisotropy in soil constitutive modeling. In: Results of the International Workshop on Constitutive Relations for Soils. Grenoble, France: A.A. Balkema; 1982b. pp. 457–62.
- Dafalias YF. On elastoplasticity-viscoplasticity constitutive modelling of cohesive soils. In: Geomechanical Modelling in Engineering Practice. Rotterdam: A.A. Balkema; 1986a. pp. 313–30.
- Dafalias YF. Bounding surface plasticity. I: mathematical foundation and the concept of hypoplasticity. *Journal of Engineering Mechanics, ASCE* 1986b;112(9):966–87.
- Dafalias YF, Herrmann LR. A bounding surface soil plasticity model. In: Proceedings of the International Symposium on Soils under Cyclic and Transient Loading. Swansea: A.A. Balkema; 1980. pp. 335–45.
- Dafalias YF, Herrmann LR. Bounding surface formulation of soil plasticity in soil mechanics transient and cyclic loads. Chichester: John Wiley and Sons, Inc.; 1982a. pp. 253–82.
- Dafalias YF, Herrmann LR. A generalized bounding surface constitutive model for clays. In: Application of Plasticity and Generalized Stress-strain in Geotechnical Engineering. New York: ASCE; 1982b. pp. 78–95.
- Dafalias YF, Herrmann LR. Bounding surface plasticity ii: application to isotropic cohesive soils. *Journal of Engineering Mechanics, ASCE* 1986;112(12):1263–91.
- Dafalias YF, Popov EP. A model of nonlinearly hardening materials for complex loadings. *Acta Mechanica* 1975;21(3):173–92.
- Dafalias YF, Popov EP. Plastic internal variables formalism of cyclic plasticity. *Journal of Applied Mechanics, ASME* 1976;98(4):645–51.
- Dafalias YF, Herrmann LR, DeNatale JS. The bounding surface plasticity model for isotropic cohesive soils and its application. In: Results of the International Workshop on Constitutive Relations for Soils, Grenoble, France. Rotterdam: A.A. Balkema; 1982. pp. 273–87.
- Dafalias YF, Manzari MT, Papadimitriou AG. Saniclay: simple anisotropic clay plasticity model. *International Journal for Numerical and Analytical Methods in Geomechanics* 2006;30(12):1231–57.
- Eisenberg MA, Phillips A. A theory of plasticity with non-coincident yield and loading surfaces. *Acta Mechanica* 1971;11(3–4):247–60.
- Fung YC. Foundations of solid mechanics. Englewood Cliffs, NJ: Prentice Hall; 1965.
- Gens A. Stress-strain and strength of a low plasticity clay. PhD Thesis. London: Imperial College, London University; 1982.
- Gudehus G. Elastoplastische Stoffgleichungen für trockenen sand. *Ingenieur-Archiv* 1973;42(3):151–69.
- Hashiguchi K, Ueno M. Elasto-plastic constitutive laws of granular materials. In: 9th International Conference on Soil Mechanics and Foundation Engineering, Constitutive Equations of Soils (specialty session 9). Tokyo, Japan: Japanese Society of Soil Mechanics and Foundation Engineering; 1977. pp. 73–82.
- Jiang J, Ling HI, Kaliakin VN. An associative and non-associative anisotropic bounding surface model for clay. *Journal of Applied Mechanics, ASME* 2012;79(3):031010. <http://dx.doi.org/10.1115/1.4005958>.
- Jiang J, Ling HI, Kaliakin VN. Simulation of natural Pisa clay using an enhanced anisotropic elastoplastic bounding surface model. *Journal of Applied Mechanics, ASME* 2013;80(2):024503. <http://dx.doi.org/10.1115/1.4007964>.
- Kaliakin VN. Bounding surface elastoplasticity-viscoplasticity for clays. PhD Thesis. Davis, California: University of California, Davis; 1985.
- Kaliakin VN. Assessment of predictive capabilities of bounding surface model for cohesive soils under complex stress paths. In: Proceedings of McMat Mechanics and Materials Conference (CD-ROM). LA, Baton Rouge; 2005.
- Kaliakin VN, Dafalias YF. Simplifications to the bounding surface model for cohesive soils. *International Journal for Numerical and Analytical Methods in Geomechanics* 1989;13(1):91–100.
- Kaliakin VN, Dafalias YF. Theoretical aspects of the elastoplastic-viscoplastic bounding surface model for cohesive soils. *Soils and Foundations* 1990a;30(3):11–24.
- Kaliakin VN, Dafalias YF. Verification of the elastoplastic-viscoplastic bounding surface model for cohesive soils. *Soils and Foundations* 1990b;30(3):25–36.
- Kaliakin VN, Nieto-Leal A. Investigation of critical states and failure in true triaxial tests of clay. In: The Second International Symposium on Constitutive Modeling of Geomaterials: advances and new applications. Heidelberg: Springer; 2012. pp. 185–91.
- Kaliakin VN, Nieto-Leal A. Towards a generalized bounding surface model for cohesive soils. In: Proceedings of the 5th Biot Conference on Poromechanics (BIOT-5). Vienna, Austria: ASCE; 2013. pp. 1011–20.
- Kaliakin VN, Pan Z. Assessment of 3-D predictive capabilities of bounding surface model for cohesive soils. In: Proceedings of the 14th U. S. National Congress on Theoretical and Applied Mechanics (CD-ROM). Blacksburg, VA; 2002.
- Kaliakin VN, Muraleetharan KK, Dafalias YF, Herrmann LR, Shinde SB. Foundation-response predictions below caisson-retained island. *Journal of Geotechnical Engineering, ASCE* 1990;116(9):1291–308.
- Krieg RD. A practical two surface plasticity theory. *Journal of Applied Mechanics, ASME* 1975;42(3):641–6.
- Ling HI, Yue D, Kaliakin VN, Themelis NJ. An anisotropic elasto-plastic bounding surface model for cohesive soils. *Journal of Engineering Mechanics, ASCE* 2002;128(7):748–58.
- Manzari MT, Nour MA. On implicit integration of bounding surface plasticity models. *Computers and Structures* 1997;63(3):385–95.
- Mróz Z, Norris VA, Zienkiewicz OC. An anisotropic hardening model for soils and its application to cyclic loading. *International Journal for Numerical and Analytical Methods in Geomechanics* 1978;2(3):203–21.
- Mróz Z, Norris VA, Zienkiewicz OC. Application of an anisotropic hardening model in the analysis of elastoplastic deformation of soils. *Geotechnique* 1979;29(1):1–34.
- Pietruszczak S, Mróz Z. Description of anisotropy of naturally k_0 -consolidated clays. In: Proceedings of the Euromechanics Colloquium, vol. 115. Villa-de-Lans, France: Kluwer Academic Publishers; 1979.
- Schofield AN, Wroth CP. Critical state soil mechanics. London: McGraw-Hill Book Co., Inc.; 1968.
- Shen CK, Sohn J, Mish K, Kaliakin VN, Herrmann LR. Centrifuge consolidation study for purposes of plasticity theory validation. In: Consolidation of Soils: Testing and Evaluation ASTM STP, vol. 892. ASTM; 1986. pp. 593–609.
- Zienkiewicz OC, Pande GN. Chapter 5: in finite elements in geomechanics. London: Wiley-Interscience; 1977. pp. 179–90.



A. Nieto-Leal earned his Bachelor Degree in Civil Engineering from Universidad Militar Nueva Granada, Bogotá, Colombia and his Master of Science in Geotechnical Engineering from Universidad de los Andes, Bogotá, Colombia. After finishing his graduate program in Geotechnical Engineering, he started working as a research assistant at Universidad Militar Nueva Granada and has been involved in teaching activities there since 2007. Currently, he is pursuing his PhD at University of Delaware supervised by Professor Victor N. Kaliakin. His research fields are computational geomechanics and constitutive modeling of geomaterials. Presently, he is studying the micro- and macroscopic response of saturated cohesive soils subjected to cyclic/dynamic loading such as earthquakes, and improving the bounding surface model to be able to better simulate such response for normally and overconsolidated soils, including post-cyclic behavior.